Oxidation Behavior of a $Zr_{52}Cu_{29}Al_{10}Ni_8$ Bulk Metallic Glass at Its Supercooled Liquid Region in the Dry Air

Haiyang Li[1,2,3,a] and Xiangxiang Gao[4,b]

[1]Luoyang Bearing Research Institute Co., Ltd., Luoyang 471039, China
[2]Henan Key Laboratory of High Performance Bearing Technology, Luoyang 471039, China
[3]Base for International Science and Technology Cooperation, Luoyang 471039, China
[4]Luoyang Non-ferrous Metal Design and Research Institute, Luoyang 471039, China
a. lihaiyang0408@outlook.com, b. 18842300943@163.com

Keywords: Oxidation, microstructure, bulk metallic glass, supercooled liquid region.

Abstract: The oxidation behavior of the $Zr_{52}Cu_{29}Al_{10}Ni_8$ bulk metallic glasses (BMGs) was studied in dry air, at its supercooled liquid region of 400 °C to 450 °C. The oxidation kinetics of the $Zr_{52}Cu_{29}Al_{10}Ni_8$ BMGs followed a multi-stage parabolic-rate law. The two-stage oxidation kinetics was obeyed at 400 °C, and 450 °C datum followed a three-stage kinetic. The parabolic-rate constants (K_p values) fluctuated with the temperature and increased with the increasing temperature. The scales formed on the BMGs were strongly dependent on the temperature, and were composed primarily of tetragonal-ZrO_2, $Cu_{10}Zr_7$, minor amounts of Cu_2O and CuO, but the disappearance of Cu_2O phase and the present of m-ZrO_2 occurred at 450 °C. Meanwhile, the Al and Ni elements were never detected in the scales at the supercooled liquid region.

1. Introduction

In recent years, amorphous alloys are widely used as structural and functional materials dependent on their good formability, excellent strength, good physical and chemical properties compared to conventional alloys[1]. And then studied on amorphous alloys have attracted increasing attention in the field of materials[2, 3]. In many amorphous alloy systems (such as Cu-, Ti-, Zr-), Zr-based bulk metallic glasses (Zr-BMGs) are ones of the most popular amorphous alloys because of their better glass forming ability[4, 5], wide liquid regions and remarkable thermal stabilities[6].

The oxidation behavior of amorphous alloys in the super cooled region has a great influence on the machining deformation of the alloy[7, 8]. Some research works on oxidation of Zr-BMGs were devoted to the oxidation kinetics and related effects of structure and composition on the oxidation resistance can be obtained from literatures[12-14]. Mao Zhang studied air oxidation of a $Zr_{55}Cu_{30}Al_{10}Ni_5$ at its super cooled liquid state, and discovered the oxidation kinetics follows a single-stage parabolic rate law at low temperatures and changes into a two-stage parabolic rate law with temperature increasing[15]. Shuaidan Lu studied the effect of yttrium addition on the air oxidation behavior of Zr-Cu-Ni-Al BMGs at 400-500 °C, and found that minor addition of Y element

can be effective in improving the oxidation-resistance of $Zr_{53.8}Cu_{29.1}Ni_{7.3}Al_{9.8}$ metallic glass[16]. However, the oxidation process is complex and the conclusions drawn from numerous studies are not uniform. Few studies have been conducted on the short-term oxidation behavior of $Zr_{52}Cu_{29}Al_{10}Ni_8$-BMG, especially the influences of oxidation time and high temperature for the oxidation order on the alloy surface are still lacking.

In this study, we mainly pay our attentions to the oxidation behavior at its super cooled liquid region in a relative short-term stage. By observing the surface morphologies and analyzing the oxidation compounds, a clear understanding of the oxidation micro-mechanism in a short time stage was achieved to study the effect of oxide constituents on the oxidation resistance at high temperature. Several experimental techniques are combined in this investigation, including X-ray diffraction (XRD), thermo-gravimetric analyzer (TGA), scanning electronic microscopy (SEM), transmission electron microscope (TEM) and differential scanning calorimeter (DSC).

2. Experiments

$Zr_{52}Cu_{29}Al_{10}Ni_8$-BMG samples were fabricated by the copper mold casting process under argon atmosphere. Samples for oxidation investigation were sliced into 10 mm×10 mm×2 mm, mechanically grinded with sandpaper followed by polishing with 2.5 μm Al_2O_3 lubricant and immediately dried before the tests. Then Samples were placed in a muffle furnace for high temperature oxidation testing. The heating time was calculated when reached the predetermined heating temperature. Then, the samples were naturally cooled in the air.

Characterization of the BMG's substrates and scales were performed by XRD (PANalytical B.V., Almelo, The Netherlands) using Philips X'pert MRD system under Cu Kα radiation (λ = 0.154 nm) from 10º to 90º and TEM (TecnaiG20, FEI, Hillsboro, OR, USA). The supercooled liquid region of the samples was characterized by using DSC (STA449 F3, NETSZCH, Germany) equipped with a thorium furnace, at a heating rate of 10K/ min.

The oxidation texts of samples were carried out under a dry air by a TGA (TGA/DSC3+, METTLER TOLEDO, Zurich, Switzerland) with the dry air (>99.99% volume percent pure) at 60ml/min. The heating profile ranged from room temperature to a pre-set temperature (between 400 ºC and 450 ºC) with a heating rate of 10K/min. The chemical compositions for the surface of the oxide scales were examined by SEM (Hitachi S-4800N, Hitachi, Japan) and energy dispersive spectroscopy (EDS, X-Max 50, OXFORD, Oxford, UK) at an accelerating voltage of 2.0 kV.

3. Results and Discussion

3.1. Alloy Characterization

The XRD spectra of the as-cast $Zr_{52}Cu_{29}Al_{10}Ni_8$-BMG shown in Figure 1, indicated that this glassy alloy only contained one wide-broadening peak near 2θ = 37.9º. And from the microscopic point of view, Figure 2 (a) showed there were no diffraction spots reflecting the crystalline phase in the bright-field image. Especially, the Figure 2 (b) showed the image contrast were uniform, the selected electron diffraction pattern consists of two strong and weak diffraction halos. The results fully revealed that the alloy had a pour amorphous structure[17-19]. DSC curve of the examined alloy was presented in Figure 3 revealed the glass transition temperature (T_g) and the onset temperature of crystallization (T_x) were 423.5 ºC and 487.6 ºC, respectively. The supercooled liquid region for the BMG (ΔT=T_x-T_g) was about 64.1 ºC, indicated a good glass forming ability of $Zr_{52}Cu_{29}Al_{10}Ni_8$. Thus, the oxidation tests of the interesting temperature were 400 ºC and 450 ºC at the supercooled liquid region[20].

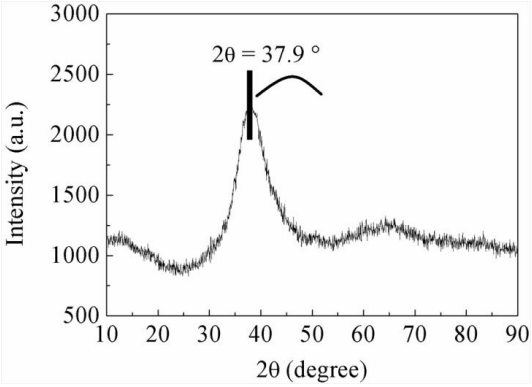

Figure 1: The XRD pattern of $Zr_{52}Cu_{29}Al_{10}Ni_8$-BMG samples prepared.

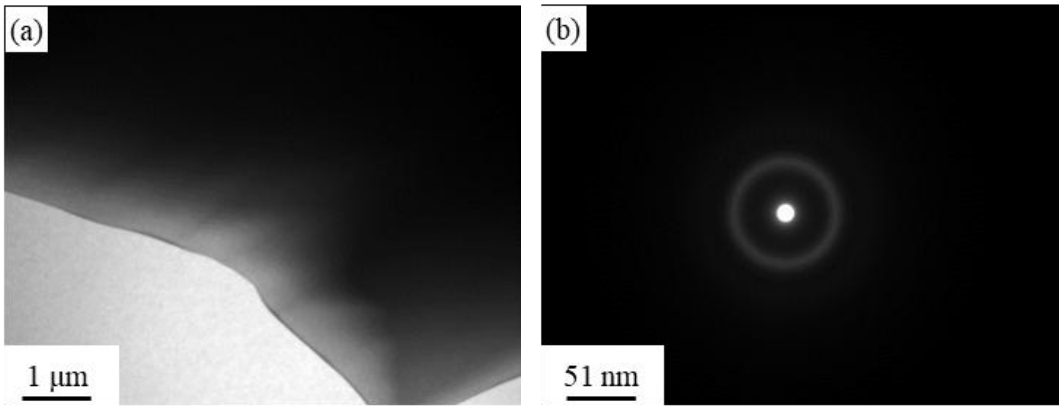

Figure 2: TEM images of the $Zr_{52}Cu_{29}Al_{10}Ni_8$-BMG samples prepared at room temperature: (a) bright-field image and (b) SAED pattern image.

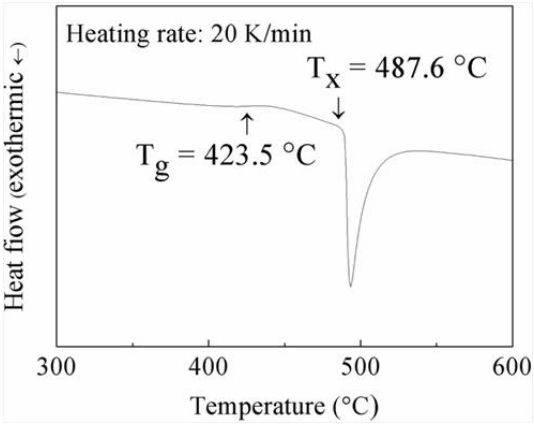

Figure 3: DSC curves of the $Zr_{52}Cu_{29}Al_{10}Ni_8$-BMG.

3.2. Oxidation Kinetics

Figure 4 showed a parabolic plot of mass gain data for the $Zr_{52}Cu_{29}Al_{10}Ni_8$-BMG over the temperature range from 400 °C to 450 °C. As shown in this figure, the oxidation kinetics of amorphous alloys generally followed the multi-step parabolic rate rule, strongly dependent on temperature. It could be seen from the figure the datum obeyed two-stage oxidation kinetics. Meanwhile, the parabolic growth was very slow before 15 minutes, and the mass growth was almost

close to zero. This period was considered as the initial slow-growth transient oxidation stage [21], and then, followed by a second steady-state stage (after 80 minutes). The K_p obtained by the fitting slope in this figure at different stages of the $Zr_{52}Cu_{29}Al_{10}Ni_8$-BMG were tabulated in Table 1. K_p increased significantly and tended to a stable value with the oxidation time increased. In addition, 450 ºC datum followed a three-stage kinetics, consisted of an initial fast growth stage (up to about 15 minutes), followed by a decreased second stage (25–60 minutes) in this stage, K_p started to change from a slow increase to a gradual decrease. It showed an upward convex shape in the figure. The increase in the mass of oxidation at this stage was the most obvious, and then, by a third steady-state stage (after 80 minutes). The observed multiple oxidation kinetics may be due to a selective oxidation present at the temperature range of interest. It was likely that when the glassy substrate initially reacts with oxygen, its amorphous structure remained unchanged at the reaction front. However, after a short period of exposure, the initial growth of the oxide scale under selective oxidation (which will be described later) happened, in turn leaded to small changes in the local substrate composition and the crystallization of the substrate. With the growth of time, the easily oxidized elements on the surface of the substrate were completely react, the formation of oxide scale further hinders the contact of oxygen with the matrix, resulted to a decrease in the parabolic-rate constant of the oxidation reaction. As for the subsequent linear growth, it may be due to the diffusion mechanism reaching a certain balance. Based on the above reasons, formed the above-mentioned various oxidation kinetics.

In addition, by comparing the mass gain curves between 400 ºC and 450 ºC, it could be seen that the parabolic-rate constants increased with temperature. The higher the temperature was, the greater the parabolic-rate constants became. This further indicated that the oxidation kinetics of the amorphous alloy was strongly dependent on temperature. And the parabolic-rate constants were positively correlated with the temperature.

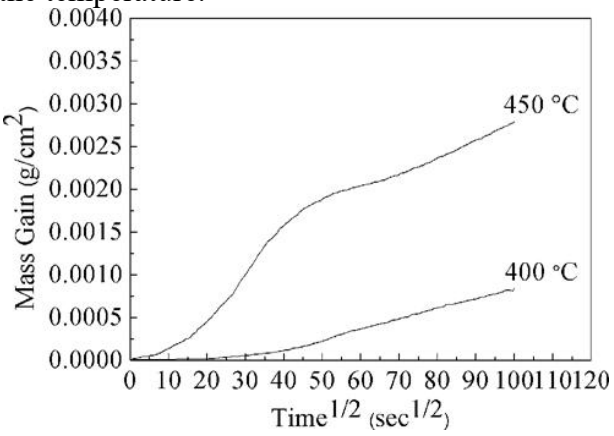

Figure 4: Parabolic plots of the mass-gain data for the $Zr_{52}Cu_{29}Al_{10}Ni_8$-BMG.

Table 1: The parabolic-rate constants of $Zr_{52}Cu_{29}Al_{10}Ni_8$-BMG for various durations at 400 °C and 450 °C (K_p unit: $g^2/cm^4/s$).

Temperature	Time				
	5 mins	10 mins	20 mins	40 mins	80 mins
400°C	5.32×10^{-14}	1.75×10^{-13}	2.75×10^{-12}	3.24×10^{-13}	4.13×10^{-10}
450°C	7.22×10^{-10}	3.36×10^{-9}	4.51×10^{-9}	5.13×10^{-13}	4.77×10^{-10}

3.3. Surface Morphologies

The surface oxidation of the $Zr_{52}Cu_{29}Al_{10}Ni_8$-BMG amorphous alloy in the supercooled liquid state for one hour at 400 °C was shown in Figure 5. The XRD results showed that the substrate surface was mainly composed of a large amount of $Cu_{10}Zr_7$ and t-ZrO_2, CuO and trace amounts of m-ZrO_2. Correspondingly, the white part of the scanning electron microscope image showed that the oxidized region was dotted on the entire surface of the substrate, indicated that the degree of oxidation of $Zr_{52}Cu_{29}Al_{10}Ni_8$-BMG was relatively low, which was consistent with the trend of the mass gain curve at 400 °C in the previous section. At 450 °C, the substrate surface was mainly composed of a large amount of t-ZrO_2, CuO and a small amount of m-ZrO_2. Meanwhile, the image of the scanning electron microscope in Fig. 6 could be seen that a large oxide scale appeared on the surface of the substrate, they were connected to each other in a sheet shape to completely cover the surface of the substrate to form a continuous oxide scale.

By comparing the surface composition of two different temperature amorphous alloy substrates, three problems worth discussing were as follows: Firstly, at 400 ºC, due to the lower oxidation rate constant at low temperature, the substrate surface did not oxidize sufficiently for over 60 minutes and the crystalline phase $Cu_{10}Zr_7$ appeared, indicated that $Zr_{52}Cu_{29}Al_{10}Ni_8$-BMG has started to crystallize at 400 ºC and the oxidation and crystallization have occurred within the same time period [22], the detailed sequence of occurrence would be fully discussed in the next section. Secondly, it was worth noting that $Cu_{10}Zr_7$ crystal phase was produced on the entire substrate surface and there were no other binary crystal phase (such as Cu_2Zr, $CuZr_2$, etc.) [23]. This may be related to the elemental ratio of Cu and Zr in the amorphous alloy or other crystalline phases but not remaining on the surface of the substrate and thus fail to be detected, specific reasons still required further experiments to verify. Thirdly, $Zr_{52}Cu_{29}Al_{10}Ni_8$-BMG contained Ni at a mass fraction of 8%, but due to the chemical stability of Ni, it did not react with oxygen to form oxides and due to the nucleation and growth ratio of Ni-Zr, Ni-Al or ternary intermetallic compounds were too slow compared with $Cu_{10}Zr_7$, so Ni was likely to be dissolved in a glassy substrate and can't be detected[24]. In addition, the Al element never appeared in the supercooled region, probably because the nucleation and growth of Al_2O_3 was too slow, causing its content to fall below the minimum detection limit of XRD and was not found, this was also the reason why the oxidation rate constant in the overcooling zone was large and the antioxidant effect was poor.

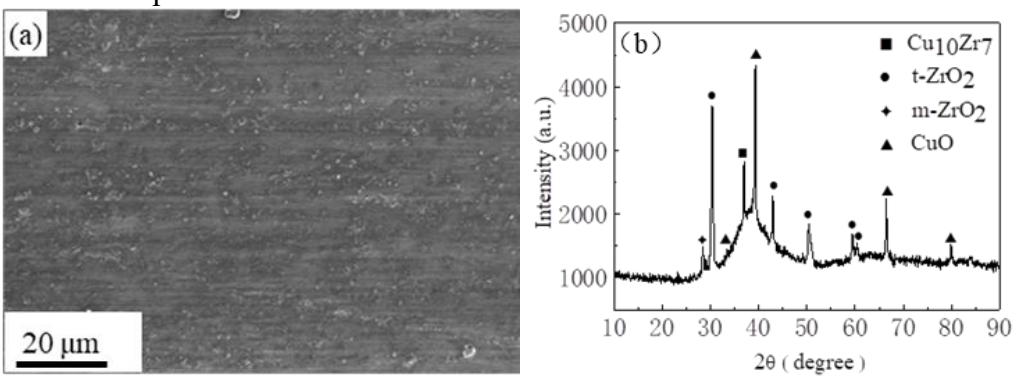

Figure 5: Surface BEI micrograph (a) and corresponding XRD spectra (b) of the $Zr_{52}Cu_{29}Al_{10}Ni_8$-BMG oxidized for 60 minutes at 400 ºC.

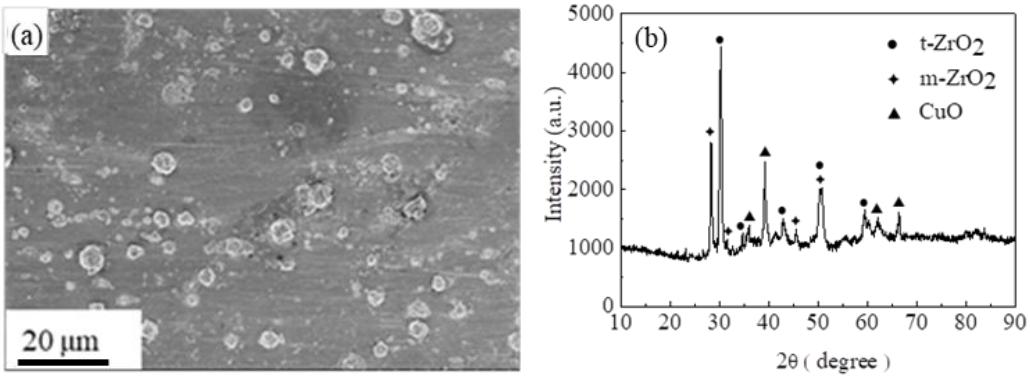

Figure 6: Surface BEI micrograph (a) and corresponding XRD spectra (b) of the $Zr_{52}Cu_{29}Al_{10}Ni_8$-BMG oxidized for 60 minutes at 450 ºC.

3.4. Short-term Oxidation

In order to understand the oxidation behavior of $Zr_{52}Cu_{29}Al_{10}Ni_8$-BMG in the supercooled liquid region, a series of short-term oxidation tests were performed at 400 and 450 °C. The typical XRD analysis of amorphous alloys after oxidation for different durations was showed in Fig. 7. When the temperature in the muffle furnace rises from room temperature to 400 °C, t-ZrO_2 and $Cu_{10}Zr_7$ appear first on the surface of the amorphous alloy. After the oxidation continued for 5 minutes, the XRD results showed that new oxides Cu_2O and CuO appeared on the surface of the substrate. The content of CuO was extremely rich and distributed over the surface of the substrate. When the amorphous alloy was exposed for 20 minutes, Cu_2O disappeared completely. After 40 minutes of continuous oxidation, the detection content of $Cu_{10}Zr_7$ began to decrease, while the content of t-ZrO_2 continued to increase throughout the entire process. Based on the detection results, it could be determined that the oxidation and crystallization of amorphous alloys took place at the same time at 400 °C. The oxidation sequence of the alloy was first selective oxidation of Zr to t-ZrO_2, followed by the growth of Cu_2O and CuO, and finally m-ZrO_2 was generated. When the oxidation temperature of the amorphous alloy was 450 °C, showed in Figure 8, t-ZrO_2, $Cu_{10}Zr_7$ and CuO were detected on the surface of the amorphous alloy. The type of compound detected by XRD was very similar to that at 400 °C, but the initial oxidation rate constant was much higher than that at 400 °C, in which t-ZrO_2 and CuO appeared in large amounts on the surface of the substrate. At 5 minutes, no new material was formed or no material disappeared, but the content of t-ZrO_2 increased with the oxidation time. At the same time, the content of $Cu_{10}Zr_7$ continues to decrease as the oxidation time increased. After 20 minutes of exposure to the amorphous alloy, the contents of t-ZrO_2 and $Cu_{10}Zr_7$ still changed according to the previous trend, but the most critical was that a small amount of m-ZrO_2 appears on the oxide scale surface. Eventually, $Cu_{10}Zr_7$ disappeared completely after 40 minutes of continuous oxidation. In contrast, the content of t-ZrO_2 and m-ZrO_2 accounted for an absolute proportion. Therefore, the order of oxidation of the amorphous alloy at 450 °C was basically the same as that at 400 °C except Cu_2O was missing.

Here the main issues worthy of discussion focused on the following areas: An interesting aspect of the first discussion was that t-ZrO_2 was first formed at 400 °C, indicated that the affinity between Zr and oxygen was the strongest compared to the other elements in the amorphous alloy, showing its first growth characteristics[25]. However, the stable temperatures were from 1200 ° C up to about 1500 ºC for t-ZrO_2, the reason why t-ZrO_2 could exist stably at 400 °C may be affected by the grain size[26]. Second, Cu_2O appears at lower temperatures, the growth rate of Cu_2O was much faster than that of CuO, thus, the formation of the high-defective Cu_2O in the oxidation of $Zr_{52}Cu_{29}Al_{10}Ni_8$-BMG

at 400 ºC was responsible for a fast reaction rate, compared to that at 450 ºC when Cu_2O was absent. The third aspect was the content of the crystalline phase $Cu_{10}Zr_7$ strongly dependent on the oxidation time and temperature, it could be seen that the initial content of $Cu_{10}Zr_7$ crystal phase was very abundant in its supercooled liquid state, but with the increase of temperature and time, the content of $Cu_{10}Zr_7$ decreased obviously and finally disappeared completely at 450 °C after 40 minutes. The reason was that the higher the temperature, the faster the oxidation rate of Cu and Zr accelerated the decomposition of the crystalline phase[27]. The last interesting aspect was m-ZrO_2, At 450 °C, m-ZrO_2 appeared for 20 minutes of oxidation and the content was positively correlated with time, while the short-term oxidation process at 400 °C did not appear at all, indicated a higher temperature could promote transformation of the crystal form of m-ZrO_2[28].

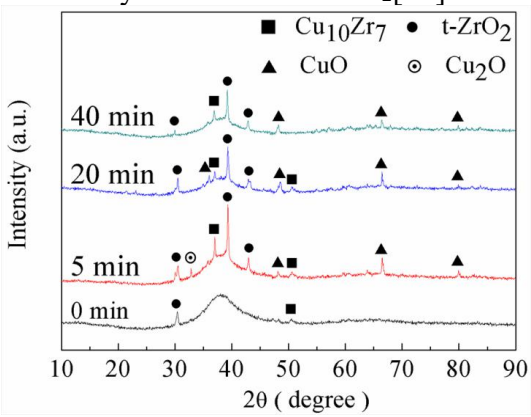

Figure 7: XRD spectra of the scales formed on the $Zr_{52}Cu_{29}Al_{10}Ni_8$-BMG oxidized at 400 ºC for various durations.

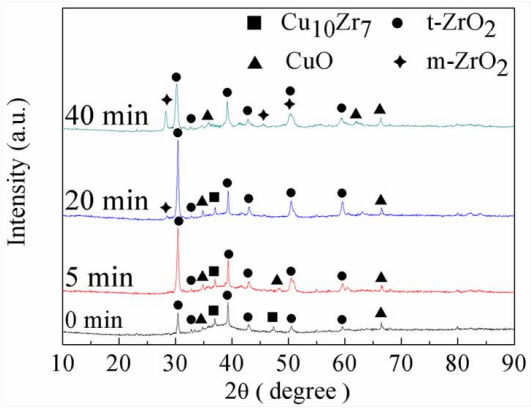

Figure 8: XRD spectra of the scales formed on the $Zr_{52}Cu_{29}Al_{10}Ni_8$-BMG oxidized at 450 °C for various durations.

4. Conclusions

The oxidation behavior of Zr52Cu29Al10Ni8 bulk metallic glass at its supercooled liquid state was characterized. Several conclusions can be reached:

The oxidation kinetics of amorphous alloys generally followed the multi-step parabolic rate rule strongly depends on temperature. The two-stage oxidation kinetics was followed at 400 ºC and 450 ºC data followed three-stage kinetics.

The compounds formed on the surface during oxidation are mainly t-ZrO_2 and CuO, with little amount of m-ZrO_2 and Cu_2O was disappeared at 450 °C.

M-ZrO_2 began to appear after 20 minutes of oxidation and the content was positively correlated with the time of oxidation at 450 °C. While the short-term oxidation process never detected at 400 °C, indicated a higher temperature could promote transformation of the crystal form of m-ZrO_2.

The Al element never detected in the super cooled liquid region, which lead to oxidation rate constant in the supercooled liquid region was large and the antioxidant effect was poor.

References

[1] D. Kawase, A.P. Tsai, A. Inoue, T. Masumoto, Crystallization on Supercooled Liquid in Metallic Zr-Cu-Al Glasses, J. SCI. Applied Physics Letters. 62.2 (1993) 137.

[2] Kai, W, Oxidation Behavior of A Zr–Cu–Al–Ni Amorphous Alloy in Air at 300–425 °C, J. SCI. Intermetallics. 10.11-12 (2002) 1265-1270.

[3] D.Y. Huang, X.J. Zhao, T. Zhang, V. Ji, Air Oxidation Kinetics Study of Zr58 Nb3Cu16Ni13Al10 Bulk Metallic Glass, J. SCI. Defect & Diffusion Forum, (2009) 209-213.

[4] W. Kai, P.C. Lin, W.S. Chen, C.P. Chuang, P.K. Liaw, H.H. Huang. H.H. Hsieh, Air Oxidation of A Zr50Cu43Al7 Bulk Metallic Glass at 400–500 °C, J. SCI. Corrosion Science, 64 (2012) 98-104.

[5] R.C. Garvie, The Occurrence of Metastable Tetragonal Zirconia as a Crystallite Size Effect, J. SCI. Journal of Physical Chemistry, 69 (1965) 1238-1243.

[6] W. Kai, H.H. Hsieh, T.H. Ho, R.T. Huang, Y.L. Lin, Air-Oxidation Behavior of a Cu 60Hf25Ti15 Bulk Metallic Glass at 375–520 °C, J. SCI. Oxidation of Metals, 68 (2007) 177-192.

[7] J. Dąbrowa, L. Perriere, M. Stygar, W. Kucza, Ł. Klita, Oxidation Behavior of Zr43Cu45Al12 Bulk Metallic Glass at 400-525 °C in Air Atmosphere, J. SCI. Journal of Materials Engineering & Performance, 24 (2015) 4863-4869.

[8] C. Y. Tam, C. HShek, W. H. Wang, Oxidation Behaviour of A Cu-Zr-Al Bulk Metallic Glass, J. SCI. Reviews on Advanced Materialsence. 18 (2008) 107-111.

[9] K. Asami, T. Moriya, T. AJr, K. Hashimoto, T. Masumoto, Oxidation Behavior of Sputter-Deposited Cu-Ta Alloys in Air, J. SCI. Materials Science & Engineering A. 226 (1997) 925-929.

[10] R. C. Garvie, The Occurrence of Metastable Tetragonal Zirconia as a Crystallite Size Effect, J. SCI. Journal of Physical Chemistry. 69 (1965) 1238-1243.

[11] A. T. Pichugin, O. H. Luk'Yanenko, V. M, Azhazha, Oxidation of Zirconium and Zr + 1% Nb Alloy in Air under Nonstationary Conditions, J. SCI. Materials Science. 36 (2000) 683-688.

[12] N. Mattern, J. Bednarcik, M Stoica, J Eckert, Temperature Dependence of The Short-Range Order of Cu65Zr35 Metallic Glass, J. SCI. Intermetallics. 32 (2013) 51-56.

[13] AInoue, T. Zhang, Fabrication of Bulk Glassy ZrAlNi5Cu Alloy of 30 mm in Diameter by a Suction Casting Method, J. SCI. Mater.trans.jim. 37 (1996) 185-187.

[14] Y. Yokoyama, E. Mund, A. Inoue, L. Schultz, Production of Zr55Cu30Ni5Al50 Glassy Alloy Rod of 30 mm in Diameter by a Cap-Cast Technique, J. SCI. Materials Transactions. 48 (2007) 1641.

[15] M. Zhang, D. Yao, X. Wang, L. Deng, Air Oxidation of A Zr55Cu30Al10Ni5 Bulk Metallic Glass at Its Super Cooled Liquid State, J. SCI. Corrosion Science. 82 (2014) 410-419.

[16] Lu S, Sun S, G. Tu, X. Huang , K. Li, The Effect of Yttrium Addition on The Air Oxidation Behavior of Zr-Cu-Ni-Al Bulk Metallic Glasses at 400-500 °C, J. SCI. Corrosion Science. 137 (2018) 53-61.

[17] L. Liu, K. C. Chan, Oxidation of Zr55Cu30Al10Ni Bulk Metallic Glass in The Glassy State and The Supercooled Liquid State, J. SCI. Applied Physics A Materials Science & Processing. 80 (2005) 1737-1744.

[18] Z. Grzesik, S. Mrowec, Kinetics and Thermodynamics of Point Defects in Non-Stoichiometric Metal Oxides and Sulphides, J. SCI. Journal of Thermal Analysis &Calorimetry. 90 (2007) 269-282.

[19] W. Kai, T. H. Ho, H. H.H.sieh, Y.R, Chen D.C, Qiao F, Jiang G, Fan P.K. Liaw, Oxidation Behavior of CuZr-Based Glassy Alloys at 400 °C to 500 °C in Dry Air, J. SCI. Metallurgical & Materials Transactions A. 39 (2008) 1838-1846.

[20] H. P. Worch, Kofstad, High Temperature Corrosion. Elsevier Applied Science, London/New York 1988, pp.546.

[21] T.A.M. Aboki, M.L. Masse, ADezellus, P. Ochin, R. Portier, First Investigations on Twin-Rolled Zr59Cu20Al10Ni8Ti3 Bulk Amorphous Alloy by Mechanical Spectroscopy, J. SCI. Materials Science & Engineering A. 370 (2004) 330-335.

[22] N. F. Mott, A Theory of The Formation of Protective Oxide Films on Metals, J. SCI. Transactions of the Faraday Society. 43 (1947) 472-483.

[23] A. I. Foster, M. L. Sims, D. Young, Protective Metal Oxide Films on Metal or Alloy Substrate Surfaces Susceptible to Coking, Corrosion or Catalytic Activity. US, 1981.
[24] I.M. Fedorchenko, É. T. Denisenko, A.V. Sakhnenko, A.P. Polushko, Effect of Temperature and Loading Rate on The Process of Deformation of Sintered Copper and Copper with Al2O3 in Air, J. SCI. Soviet Powder Metallurgy & Metal Ceramics. 15 (1976) 887-892.
[25] F. Gesmundo, B. Gleeson, Oxidation of Multicomponent Two-Phase Alloys, J. SCI. Oxidation of Metals. 44 (1995) 211-237.
[26] C. Michaelsen, C. Gente, R. Bormann, The Thermodynamics of Amorphous Phases in Immiscible Systems: The Example of Sputter-Deposited Nb–Cu Alloys, J. SCI. Journal of Applied Physics. 81 (1997) 6024-6030.
[27] R. C. Garvie, The Occurrence of Metastable Tetragonal Zirconia as a Crystallite Size Effect, J. SCI. Journal of Physical Chemistry. 69 (1965) 1238-1243.
[28] C. Y. Tam, C. HShek, Oxidation Behavior of Cu60Zr30Ti10 Bulk Metallic Glass, J. SCI. Journal of Materials Research. 20 (2005) 1396-1403.